Available online at www.sciencedirect.com

ScienceDirect

Procedia Engineering 199 (2017) 1429–1434

Procedia Engineering

www.elsevier.com/locate/procedia

X International Conference on Structural Dynamics, EURODYN 2017

A systematic approach to derive dynamic equations for homogeneous and functionally graded micropolar plates

Hossein Abadikhah, Peter D. Folkow*

Dept. of Applied Mechanics, Chalmers University of Technology, 412 96 Gothenburg, Sweden

Abstract

This work considers a systematic derivation process to obtain hierarchies of dynamical equations for micropolar plates being either homogeneous or with a functionally graded (FG) material variation over the thickness. Based on the three dimensional micropolar continuum theory, a power series expansion technique of the displacement and micro-rotation fields in the thickness coordinate of the plate is adopted. The construction of the sets of plate equations is systematized by the introduction of recursion relations which relates higher order powers of displacement and micro-rotation terms with the lower order terms. This results in variationally consistent partial differential plate equations of motion and pertinent boundary conditions. Such plate equations can be constructed in a systematic fashion to any desired truncation order, where each equation order is hyperbolic and asymptotically correct. The resulting lowest order flexural plate equation is seen to be of a generalized Mindlin type. The numerical results illustrate that the present approach may render accurate solutions of benchmark type for both homogeneous and functionally graded micropolar plates provided higher order truncations are used. Moreover, low order truncations render new sets of plate equations that can act as engineering plate equations, e.g. of a generalized Mindlin type.

Peer-review under responsibility of the organizing committee of EURODYN 2017.

Keywords: Eigenfrequency; Series expansion; Recursion relations; Variationally consistent; Asymptotic correct

1. Theory of linear micropolar elasticity

Consider an isotropic micropolar continuum according to Eringen's theory [1]. The equations of balance of momentum and moment of momentum, written in cartesian coordinates, are expressed as

$$t_{kl,k} = \rho \ddot{u}_l, \tag{1}$$

$$m_{kl,k} + \epsilon_{lkm} t_{km} = \rho j_{lk} \ddot{\phi}_k, \tag{2}$$

* Peter D. Folkow. Tel.: +460-31-772-1521.
E-mail address: peter.folkow@chalmers.se

1877-7058
Peer-review under responsibility of the organizing committee of EURODYN 2017.
10.1016/j.proeng.2017.09.389

in absence of body forces and body couples. Here t_{kl} is the stress tensor, m_{kl} is the couple stress tensor, u_l is the displacement vector, ϕ_k is the micro-rotation vector, ρ is the density, j_{lk} is the microinertia tensor and ϵ_{lkm} is the permutation symbol. Indices that follow a comma indicate partial differentiation. The surface tractions are defined in accordance to

$$t_l = t_{kl} n_k, \tag{3}$$

$$m_l = m_{kl} n_k, \tag{4}$$

where n_k is an outward pointing normal surface vector. The micropolar strain tensors ε_{kl} and γ_{kl} are defined by

$$\varepsilon_{kl} = u_{l,k} + \epsilon_{lkm}\phi_m, \tag{5}$$

$$\gamma_{kl} = \phi_{k,l}. \tag{6}$$

These strain measures are related to the stress and couple stress tensors through the constitutive relations

$$t_{kl} = \lambda\varepsilon_{mm}\delta_{kl} + (\mu + \kappa)\varepsilon_{kl} + \mu\varepsilon_{lk}, \tag{7}$$

$$m_{kl} = \alpha\gamma_{mm}\delta_{kl} + \beta\gamma_{kl} + \gamma\gamma_{lk}, \tag{8}$$

where δ_{kl} is the Kronecker delta, λ and μ are Lamé parameters while α, β, γ and κ are micropolar elastic moduli. Consider from now on spin-isotropic materials where the microinertia reduces to a scalar quantity, $j_{kl} = j\delta_{kl}$.

2. Series expansion, recursion relations and plate equations

The governing equations for a micropolar continuum as described above are to be applied to a homogenous or FG isotropic plate of thickness $2h$. A cartesian coordinate system $\{x, y, z\}$ is used, where the in plane x and y axes are along the middle plate plane at $z = 0$. The components of the displacement field and micro-rotation field are denoted $\{u_1, u_2, u_3\}$ and $\{\phi_1, \phi_2, \phi_3\}$ respectively. The derivation procedure of the plate equations is based on the assumption that each component of the displacement field and micro-rotation field can be expanded in a power series in the thickness coordinate z according to

$$u_l(x, y, z, t) = \sum_{n=0}^{\infty} z^n u_l^{(n)}(x, y, t), \tag{9}$$

$$\phi_l(x, y, z, t) = \sum_{n=0}^{\infty} z^n \phi_l^{(n)}(x, y, t). \tag{10}$$

Using the assumptions in Eqs. (9) and (10), the constitutive equations (7) and (8), as well as the deformation relations Eqs. (5) and (6), it is possible to express all the stress and couple stress components in power series form

$$t_{kl} = \sum_{n=0}^{\infty} z^n t_{kl}^{(n)}, \tag{11}$$

$$m_{kl} = \sum_{n=0}^{\infty} z^n m_{kl}^{(n)}. \tag{12}$$

For the homogeneous case

$$t_{kl}^{(n)} = \lambda L_i u_i^{(n)}\delta_{kl} + \mu(L_l u_k^{(n)} + L_k u_l^{(n)}) + \kappa(L_k u_l^{(n)} + \epsilon_{lkm}\phi_m^{(n)}), \tag{13}$$

$$m_{kl}^{(n)} = \alpha L_i \phi_i^{(n)} \delta_{kl} + \beta L_l \phi_k^{(n)} + \gamma L_k \phi_l^{(n)}, \tag{14}$$

while a similar albeit slightly more complicated relation holds for FG material using that the material parameters vary in the thickness direction. In that FG case these fields are expanded in Taylor series [7] as

$$f(z) = \sum_{n=0}^{\infty} z^n f^{(n)}, \tag{15}$$

where f covers both traditional elastic parameters $\{\rho, \lambda, \mu\}$ and the micropolar parameters $\{\kappa, \alpha, \beta, \gamma, j\}$. Note that the introduced operator L_k is defined as

$$L_k f_l^{(n)} = \begin{cases} \partial_x f_l^{(n)} & \text{if } k = 1, \\ \partial_y f_l^{(n)} & \text{if } k = 2, \\ (n+1) f_l^{(n+1)} & \text{if } k = 3, \end{cases} \tag{16}$$

where ∂_x and ∂_y are used to denote partial derivatives with respect to x and y.

2.1. Recursion relations

By inserting the expanded displacement and micro-rotation fields Eqs. (9) and (10), together with the expanded stress and couple stress tensors Eqs. (11) and (12) into the equations of motion, Eqs. (1) and (2), and collecting terms of equal power in z one can obtain recursion formulas for each displacement and micro-rotation field. The recursion formulas are essential for the derivation of the plate equations since the number of expansion functions for each field can be reduced from an infinite amount to a finite amount. By using the recursion formulas it is possible to express all expansion functions $u_l^{(n)}$ and $\phi_l^{(n)}$ with $n = \{2, 3, \dots\}$ in terms of the lowest order ones with $n = \{0, 1\}$. For the homogeneous case the recursion formulas are obtained as

$$\begin{aligned} &(\mu+\kappa)(n+2)(n+1)u_l^{(n+2)} + (\lambda+\mu)(n+2)(n+1)u_3^{(n+2)}\delta_{3l} = \\ &\rho \ddot{u}_l^{(n)} - (\mu+\kappa)(\partial_x^2 + \partial_y^2)u_l^{(n)} - (\lambda+\mu)L_l(\partial_x u_1^{(n)} + \partial_y u_2^{(n)} \\ &+ (n+1)u_3^{(n+1)}(1-\delta_{3l})) - \kappa\delta_{li}\epsilon_{ijk}L_j\phi_k^{(n)}, \quad n = 0, 1, \dots, \end{aligned} \tag{17}$$

$$\begin{aligned} &\gamma(n+2)(n+1)\phi_l^{(n+2)} + (\alpha+\beta)(n+2)(n+1)\phi_3^{(n+2)}\delta_{3l} = \\ &\rho j \ddot{\phi}_l^{(n)} - \gamma(\partial_x^2 + \partial_y^2)\phi_l^{(n)} - (\alpha+\beta)L_l(\partial_x \phi_1^{(n)} + \partial_y \phi_2^{(n)} \\ &+ (n+1)\phi_3^{(n+1)}(1-\delta_{3l})) - \kappa(\delta_{li}\epsilon_{ijk}L_j u_k^{(n)} - 2\phi_l^{(n)}), \quad n = 0, 1, \dots, \end{aligned} \tag{18}$$

for $l = 1, 2, 3$. Note that these coupled six recursion formulas do not involve any approximations since they stem from the equations of motion, Eqs. (1) and (2), and the power series expansion of the displacement and micro-rotation fields Eqs. (9) and (10). Furthermore, the power series have not been truncated which is essential for the present method. Similar but more complicated expressions are obtained for the FG case.

2.2. Plate equations

By adopting the free plate boundary condition at the surfaces at $z = \pm h$, Eqs. (11) and (12) at an order $N > 0$, gives

$$\sum_{n=0}^{N} (\pm h)^n t_{3l}^{(n)}(x, y, t) = 0, \qquad \sum_{n=0}^{N} (\pm h)^n m_{3l}^{(n)}(x, y, t) = 0. \tag{19}$$

These boundary conditions constitute the hyperbolic set of twelve partial differential equations for a micropolar plate. Using the recursion relations Eqs. (17) and (18) these plate equations may be written in terms of the twelve lowest order expansion functions $\{u_l^{(n)}, \phi_l^{(n)}\}$ for $n = \{0, 1\}$.

3. Properties of FG materials

For a FG plate the material parameters are to vary continuously over the thickness. Consider a plate where the top $z = h$ (subscript t) and the bottom $z = -h$ (subscript b) consists of different material. There are different ways to model the variation of the materials over the thickness, e.g. adopting a power law or an exponential law. Here consider the often used power law where the volume fraction of the bottom material varies as

$$V_b(z) = ((h - z)/2h)^p \,. \tag{20}$$

Note that the volume fraction law follows $V_b + V_t = 1$, and the power index p is a positive number. There are various methods to model the effective material properties in FG materials. Here consider the Voigt model for the density and the micro parameters $\{\kappa, \alpha, \beta, \gamma, j\}$, where these various material properties (denoted by Q) are assumed to be proportional to the volume ratio according to

$$Q(z) = Q_b V_b(z) + Q_t V_t(z). \tag{21}$$

As for the elastic Lamé parameters λ and μ the Mori-Tanaka model is used [8].

4. Numerical results

The object for the numerical results is to illustrate the accuracy of the present partial differential equations for homogeneous or FG micropolar plates; both for low and high order sets. The low order cases may be used as approximate engineering plate theories while the higher order theories act as benchmark theories converging to the exact 3D solution. The plates are simply supported with with free lateral surfaces. As for the FG plate the top material consists of pure aluminum, while the bottom material consists of epoxy containing randomly distributed aluminum particles. Consequently, the amount of aluminum decreases continuously from the top to the bottom of the plate. From [2] the material parameters for aluminum at the top are $E_t = 70.85$ GPa, $\nu_t = 0.33$, $\rho_t = 2800$ kg/m^3, $j_t = 0.325 \times 10^{-7}$ m^2, $\kappa_t = 1.3155 \times 10^{-5}$ GPa, $\alpha_t = 1.2355$ kN, $\beta_t = 0.1585$ kN, $\gamma_t = 0.59664$ kN while for the epoxy matrix with aluminum particles at the bottom one has $E_b = 5.31$ GPa, $\nu_b = 0.40$ $\rho_b = 2192$ kg/m^3, $j_b = 1.96 \times 10^{-7}$ m^2, $\kappa_b = 1.3234 \times 10^{-4}$ GPa, $\alpha_b = 83.255$ N, $\beta_b = 0.1028$ kN, $\gamma_b = 3.3349$ kN. As for the homogeneous plate aluminium is used throughout.

In this section, eigenfrequencies and mode shapes as well as stress distributions are illustrated for a square plate $a = b$ for a plate of thicknesses $a/h = 20$. For the FG plate the influence from the material distribution is studied by choosing different power indexes p from Eq. (20). For both the homogeneous and FG plate the lowest eigenfrequencies ω_{mn} are calculated using different truncation orders, where m and n refer to the mode numbers in the x and y directions, respectively. For convenience, introduce the non dimensional frequency $\Omega_{mn} = 1000\, \omega_{mn} h/c_t$, where the velocity c_t is for the aluminum material and defined as $c_t = \sqrt{E_t/\rho_t}$.

4.1. Eigenfrequencies

For the *homogeneous* plate it is possible to obtain exact analytical results from 3D theory; these are used as a benchmark for the approximate theories. Besides the present theory for different truncation orders, the approximate plate theories due to Eringen [3] and Sargsyan and Sargsyan [4] are also studied. Table 1 presents the eigenfrequencies for various modes. It is clear that the approximate theories due to Eringen,

Sargsyan and the present $N = 3$ theory render reasonably accurate results, even though the results for the $N = 3$ theory are slightly less accurate. The results for Eringen and Sargsyan differ for other boundary conditions not presented here [5]. As expected, the accuracies for all these approximate theories decrease as the mode numbers increase. For higher truncation orders, the results for the present theory converge rapidly to the exact eigenfrequencies.

Table 1. The eigenfrequencies Ω_{mn} for a homogeneous plate using exact theory and approximate theories.

m	n	Exact	Eringen	Sargsyan	$N = 3$	$N = 5$	$N = 7$	$N = 33$
1	1	7.48031	7.48644	7.48644	7.46805	7.48031	7.48031	7.48031
2	1	18.4555	18.4923	18.4923	18.4003	18.4555	18.4555	18.4555
2	2	29.1609	29.2468	29.2468	29.0322	29.1609	29.1609	29.1609
3	1	36.1569	36.2918	36.2918	35.9545	36.1569	36.1569	36.1569

For the *functionally graded* plate it is not possible to derive analytical 3D solutions. Here a higher order truncation ($N = 50$) is used as benchmark result. By studying the higher truncation orders more in detail, it is seen that the results for these highest presented order seem to be accurate to all the given figures. Hence, these eigenfrequencies may be used as benchmark results to the exact 3D theory [7]. It should be stressed that the present derivation process, when applied to other materials presented in the literature, render consistent numerical results for homogeneous micropolar plates [5] as well as for functionally graded elastic plates [7]. The results are given in Table 2 for different truncation orders. Note that higher eigenfrequencies are obtained for the less slender plate as expected. Moreover the eigenfrequencies become higher by increasing the power index p, as this results in higher amount of the aluminum phase. This could be compared to the homogeneous aluminum plate in Table 1 which corresponds to $p \to \infty$.

Table 2. The eigenfrequencies Ω_{mn} for a FG plate using different truncation orders.

p	mn	$N = 2$	$N = 3$	$N = 4$	$N = 6$	$N = 10$	$N = 25$	$N = 50$
	11	6.13441	4.15222	4.74982	4.61891	4.61086	4.61055	4.61055
1	12	15.0702	10.2634	11.7483	11.4193	11.3983	11.3976	11.3976
	22	23.7129	16.2477	18.6047	18.0746	18.0405	18.0396	18.0396
	11	7.54932	5.31461	5.16915	5.19175	5.21619	5.21527	5.21527
2	12	18.5484	13.1313	12.8064	12.8472	12.9082	12.9060	12.9057
	22	29.1893	20.7766	20.3105	20.3523	20.4498	20.4461	20.4461
	11	8.30785	6.29905	4.97666	5.69495	5.58045	5.57178	5.57178
3	12	20.4123	15.5434	12.3465	14.0907	13.8122	13.7914	13.7911
	22	32.1235	24.5605	19.6071	22.3193	21.8854	21.8529	21.8523
	11	8.91844	7.27265	5.54764	5.83391	5.9806	6.01247	6.01216
5	12	21.9117	17.9201	13.7509	14.4398	14.8006	14.8786	14.8777
	22	34.4817	28.2758	21.8189	22.8804	23.4507	23.5721	23.5702

4.2. Eigenmodes

In order to further illustrate the differences between the truncation orders, various plots on mode shapes and stress distributions are compared. Consider only the FG case with $p = 3$ for the fundamental frequency Ω_{11} using a thicker plate $a/h = 8$. Fig. 1 shows the displacements in the y- and z-directions, u_2 and u_3, respectively. It is clearly seen that the fundamental mode is predominately flexural, as the u_2 field is close to antisymmetric and the u_3 field is close to symmetric with respect to z. The results from $N = 3$ and $N = 4$ are almost overlapping, while the $N = 10$ curve is indistinguishable from the high order benchmark curve $N = 50$. This latter conformity for the higher modes are visible in other cases.

Next consider the normal stresses in Fig. 2. Here the differences among the truncation orders are more pronounced when compared to the displacements and the eigenfrequencies. Note that the second order polynomial used in the $N = 2$ case for the normal stress t_{33} in Fig. 2(b) does not capture the higher order

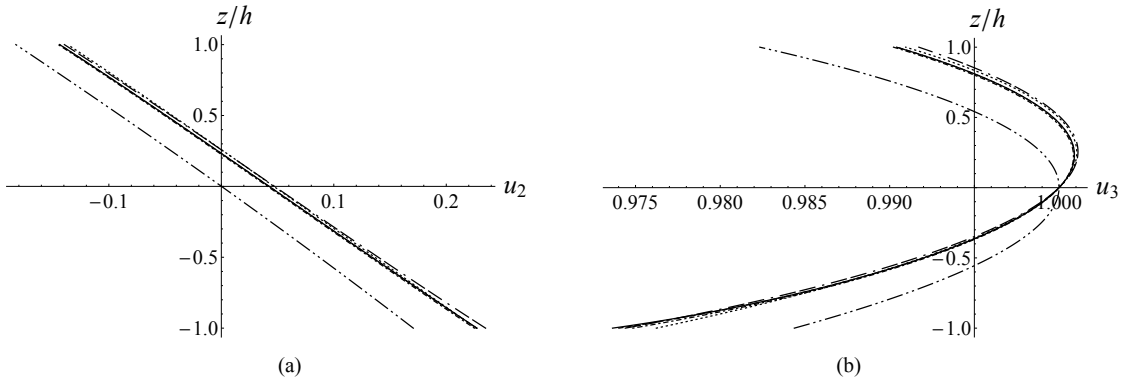

Figure 1. Displacement in y-direction u_2 (a) and z-direction u_3 (b) for the first mode: —— $N = 50$, - - - $N = 10$, - · - $N = 6$, – – · – – $N = 4$, · · · $N = 3$, – · · – $N = 2$

variation over the thickness properly. All truncation orders fulfill the stress free boundary condition at the free surfaces $z = \pm h$ as illustrated in Fig. 2(b).

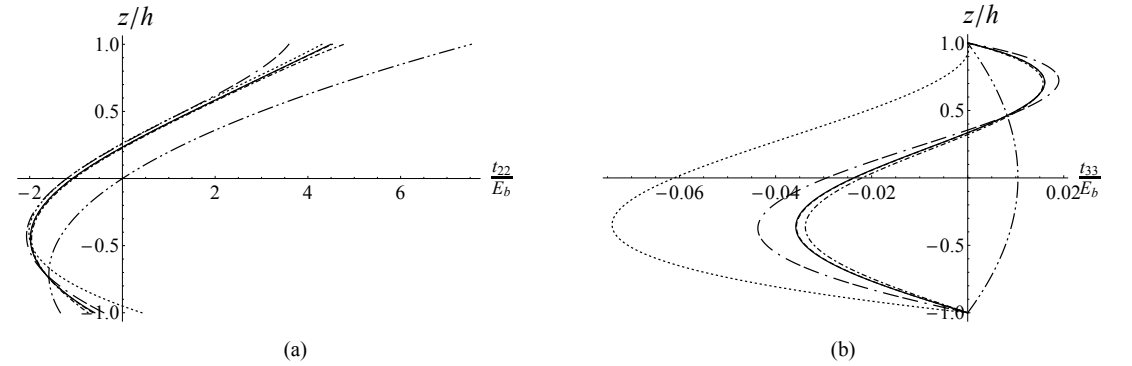

Figure 2. Normal stresses in y-direction t_{22} (a) and the z-direction t_{33} (b) for the fundamental eigenfrequency: —— $N = 50$, - - - $N = 10$, - · - $N = 6$, – – · – – $N = 4$, · · · $N = 3$, – · · – $N = 2$

References

[1] Eringen AC. Microcontinuum Field Theories Vol I Foundations Solids. Springer, 1999.
[2] A. Kiris, E. Inan, On the identification of microstretch elastic moduli of materials by using data on plates. Int. J. Eng. Sci. 46 (2008) 585–597.
[3] A.C. Eringen, Theory of miropolar plates. Z. Angew. Math. Phys. 18 (1967) 12–30.
[4] S.H. Sargsyan, A.H. Sargsyan, General dynamic theory of micropolar elastic thin plates with free rotation and special features of their natural oscillations. Acoust. Phys. 57 (2011) 473–481.
[5] Abadikhah H, Folkow PD. A hierarchy of dynamic equations for micropolar plates. J. Sound Vib. 357 (2015) 427–436.
[6] Abadikhah H, Folkow PD. A rational derivation of dynamic higher order equations for functionally graded micropolar plates. Compos Struct 153 (2016) 234–241.
[7] S.S. Vel, R.C. Batra, Three-dimensional exact solution for the vibration of functionally graded rectangular plates. J. Sound Vib. 272 (2004) 703–730.
[8] Mori T, Tanaka T. Average stress in matrix and average elastic energy of materials with misfitting inclusions. Acta Metall 21 (1973) 571–574.